# The Spiral Ganglion and Rosenthal's Canal in Beluga Whales

**Jennifer D. Sensor,[1]* Robert Suydam,[2] John C. George,[2] M. C. Liberman,[3,4] Denise Lovano,[1] Mary Ann Rhaganti,[5] Sharon Usip,[1] Christopher J. Vinyard,[1] and J. G.M. Thewissen[1]**

[1]*Department of Anatomy and Neurobiology, Northeast Ohio Medical University, Rootstown, Ohio 44240*
[2]*Department of Wildlife Management, North Slope Borough, Barrow, Alaska 99723*
[3]*Department of Otology and Laryngology, Harvard Medical School, Boston, Massachusetts 02115*
[4]*Eaton-Peabody Laboratories, Massachusetts Eye and Ear Infirmary, Boston, Massachusetts 02114*
[5]*Department of Anthropology, Kent State University, Kent, Ohio 44240*

*ABSTRACT* With the increase of human activity and corresponding increase in anthropogenic sounds in marine waters of the Arctic, it is necessary to understand its effect on the hearing of marine wildlife. We have conducted a baseline study on the spiral ganglion and Rosenthal's canal of the cochlea in beluga whales (*Delphinapterus leucas*) as an initial assessment of auditory anatomy and health. We present morphometric data on the length of the cochlea, number of whorls, neuron densities along its length, Rosenthal's canal length, and cross-sectional area, and show some histological results. In belugas, Rosenthal's canal is not a cylinder of equal cross-sectional area, but its cross-section is greatest near the apex of the basal whorl. We found systematic variation in the numbers of neurons along the length of the spiral ganglion, indicating that neurons are not dispersed evenly in Rosenthal's canal. These results provide data on functionally important structural parameters of the beluga ear. We observed no signs of acoustic trauma in our sample of beluga whales. J. Morphol. 000:000–000, 2015. © 2015 Wiley Periodicals, Inc.

KEY WORDS: Cetacea; Odontoceti; *Delphinapterus leucas*; hearing; cochlea; inner ear

## INTRODUCTION

The ear of the mammalian order Cetacea (whales, dolphins, and porpoises) is adapted for underwater hearing, and a range of frequency specializations occurs among different cetaceans. Mysticetes (baleen whales) use low-frequency sounds for long-distance communication and spatial orientation, whereas odontocetes, (toothed whales, which includes dolphins and porpoises) use high frequencies to echolocate and have complex communication repertoires (Wartzok and Ketten, 1999). The anatomy of these vastly different auditory specializations is intrinsically interesting but it is difficult to study hearing in cetaceans. Many cetaceans are large, hard to take samples from in the wild, and husbandry is difficult or impossible. In addition, there are legal (U.S. and international) and ethical issues surrounding the acquisition of fresh samples. However, some arctic cetaceans are harvested by Alaskan Native populations under subsistence-hunting provisions of the law, and necropsy material provides a unique source of fresh samples. Here, we use this material to study the cochlear morphology of wild belugas (*Delphinapterus leucas*) as a baseline for future studies on hearing in cetaceans. The increase of human activity and corresponding increase in anthropogenic sounds in the Arctic is known to affect arctic marine wildlife in the short term (Stocker, 2011), but our study is interested in permanent, long-term damage. Establishing a baseline for healthy beluga ear anatomy can provide insights into the impact of potential future acoustic exposures.

Beluga whales live in the subarctic and Arctic often near the edge of the frozen ocean. Some populations migrate north and south with the annual waxing and waning of the ice. They have one of the largest vocal repertoires within odontocetes (Bel'kovitch and Sh'ekotov, 1990). Belugas produce around 50 different emotive and communicative call types within the frequency range of 0.1–12 kHz (O'Corry-Crowe, 2009) and are also capable of vocal learning and imitation (Vergara and Barrett-Lennard, 2008). Their echolocation frequencies are much higher; Au et al. (1988) found peak echolocation frequencies to be variable but

Contract grant sponsors: North-Slope Borough, North Slope Borough School District, Kent State University School of Biomedical Science, NEOMED, and the NSB-Shell Baseline Studies Program.

*Correspondence to: J. D. Sensor; Department of Anatomy and Neurobiology, Northeast Ohio Medical University, Rootstown, OH 44240. E-mail: jsensor@neomed.edu

Received 25 April 2015; Revised 3 June 2015;
Accepted 5 July 2015.

Published online 00 Month 2015 in
Wiley Online Library (wileyonlinelibrary.com).
DOI 10.1002/jmor.20434

with a primary high near 40 kHz. Most audiograms for wild Alaskan beluga indicate high sensitivity between approximately 30–100 kHz. This is based on auditory evoked potentials (Klishin et al., 2000; Castellote et al., 2014), but behavioral audiograms (on captive individuals) are consistent with this (Finneran et al., 2005).

The purpose of this article is to document the morphology of the beluga cochlea, in particular those features that are important in hearing. Such anatomical studies on wild animals can complement functional studies on captive specimens. Laboratory studies on acoustic trauma often focus on the organ of Corti, since it transduces sound. However, because our samples came from individuals that were hunted, organs of Corti are not usable for our study for the following reason. Acoustic trauma to the organ of Corti can be immediate upon exposure (e.g., Ohlemiller et al., 2000; Wang et al., 2002; Abrashkin et al., 2006; Henderson et al., 2008), and blast damage to the ear has been documented in detail in domesticated animals (Roberto et al., 1989). Instead of the organ of Corti, we study the spiral ganglion and Rosenthal's canal in order to gain insight in the functional parameters of the cochlea and to provide a baseline for beluga hearing during life. Neurons in the spiral ganglion are susceptible to cell death when their peripheral connections with inner and outer hair cells (within the organ of Corti) die (Hurley et al., 2007; Henderson et al., 2008). This neural degeneration is not immediate. Spiral ganglion damage arises slowly; neuron death can be documented based on histological data no sooner than several weeks after the death of the hair cells (Lurie et al., 1944; Fredelius, 1988; Fredelius et al., 1988), although minor signs of damage (e.g., vacuoles in the ganglion) can be seen within several hours after exposure (Wang et al., 2002).

One objective of our study is to estimate the total number of neurons in the spiral ganglion, and we compare absolute counts of spiral ganglion cells along the cochlea to density estimates of these cells. Neuron counts in the spiral ganglion have been estimated in a variety of ways. Firbas et al. (1970) explored variation in the spiral ganglion in the guinea pig on regular tangential sections, using two methods. First, these authors counted numbers of nuclei of all neurons in all sections and reported these with a mathematical correction factor. Second, they calculated cell densities, as opposed to cell numbers, per whorl of the cochlea. They justified the use of densities on the basis of three considerations: it is less expensive since not all sections are counted, it is less in need of mathematical corrections, and it avoids the need to determine exact borders between whorls. Most modern studies have used only densities at the midmodiolar sections to evaluate the health of the ganglion cell population of the spiral ganglion (Dazert et al., 1996; Ruijven et al., 2004; Shepherd et al., 2005; Agterberg et al., 2010). Others have determined neuron densities along Rosenthal's canal and used this to calculate an estimate of neuron numbers (Wicke and Firbas, 1970; Keithley and Feldman, 1979; Schuknecht, 1993). Keithley and Feldman (1979) indicated that this would correct for oblique sectioning. When only density estimates are used to evaluate the spiral ganglion over its length, however, information regarding changes in cross-sectional area of Rosenthal's canal is lost. Johnson et al. (2011) showed that larger canal cross-sections match areas of higher neuron numbers in mice, resulting in similar neuron density numbers in spite of higher neuron numbers. Consistent with this, Richter et al. (2011) found that, in gerbils, neuron numbers in the spiral ganglion as well as Rosenthal's canal cross-sectional area increase toward the cochlear apex and that in ontogeny packing densities of neurons change.

There is some evidence that cross-sectional areas of Rosenthal's canal and numbers of spiral ganglion neurons along the length of the cochlea are variable in cetaceans too. Wever et al. (1971c) found that neuron densities drop toward the apex of the cochlea in the dolphin *Tursiops truncatus*. Broadly speaking, the spiral ganglion cells innervate adjacent parts of the hair cell bands, although the spatial correlation is complicated at the ends of the spiral, where the peripheral axons of spiral ganglion cells fan out to reach their most apical and basal targets. Thus, over much of the spiral ganglion, cell distribution can be used to evaluate innervation density and thereby infer limits on the frequency resolving power of the inner ear in different parts of the hearing range.

There has been some research on the cochlea of belugas. Solntseva (2007) published a number of images of the developing beluga labyrinth, and Ketten (1997) listed in a table that the spiral ganglion of belugas has a neuron density of 3,557 cells/mm, with an overall total estimate of 149,386 cochlear ganglion cells. There are several estimates of fiber number in the statoacoustic nerve (CN VIII) of belugas, Morgane and Jacobs (1972) estimated 171,100, whereas Jansen and Jansen (1969) estimated 210,000. However, the statoacoustic nerve not only includes fibers from afferent spiral ganglion neurons, but also efferent fibers to the cochlea, as well as fibers to and from the vestibular organ. Gao and Zhou (1991) compared the composition of the statoacoustic nerve of the cetaceans Baiji (*Lipotes vexillifer)* and finless porpoise (*Neophocaena phocaenoides)*. They found that both the ratio of spiral ganglion neuron count to cochlear fibers (*Lipotes*, 0.69; *Neophocaena*, 0.94) and the ratio of cochlear fibers to total statoacoustic nerve fibers (*Lipotes*, 0.75; *Neophocaena* 0.98) varied greatly between these species. The ratio of

cochlear fibers to total statoacoustic nerve fibers in *Tursiops* is 0.6 (Morgane and Jacobs, 1972). This indicates that it is unwise to estimate spiral ganglion counts in beluga based on assumptions about the fiber composition of this nerve in other cetaceans.

The other objectives of this study are to report on cell densities along the cochlea, cochlear length, Rosenthal's canal length, number of cochlear whorls, and show histological results to establish a baseline in beluga cochlear morphology.

## MATERIALS AND METHODS

### Specimen Acquisition

Subsistence hunting of beluga whales takes place in the village of Point Lay, Alaska, and health-related sampling of these whales occurs 3–24 h after death and is overseen by the Department of Wildlife Management, North-Slope Borough, Alaska. Samples were acquired under NOAA-NMFS permit 814-1899-03. Belugas are protected under several U.S. laws, and this makes acquisition of all types of samples under controlled conditions impossible, since samples can only be collected after subsistence harvest. Methods commonly used to study the inner ear in laboratory, domestic, or even most wild animals cannot be used here, and we modified these to adapt to the conditions present.

To remove a periotic bone from the skull, we approach the ear ventrally, removing parts of the hyoid arch. This exposes the ventral side of the tympanic bulla. Rongeurs are used to open the middle ear cavity, and the tympanic, malleus, and incus are removed. The stapes is firmly attached in the oval window and is not dislodged in this process. The periotic is only loosely attached to the skull on its caudal side, and is unattached by bone otherwise. We use a scalpel to resect soft-tissue connections rostral, lateral, and medial, and then use rongeurs to extract the periotic. The periotic is immediately submerged in 2.5% glutaraldehyde (a common fixative for the organ of Corti, Wang et al., 2002), and postfixed for at least 3 weeks. After fixation, specimens are stored in 1x PBS.

Specimens are cataloged in the collection of the North Slope Borough, Department of Wildlife management. Specimens numbers indicate the year caught (e.g., 2010), a locality and species acronym (LDL, Point Lay, *D. leucas*), and a rank order number (e.g., 10), yielding 2010LDL10. Table 1 provides information about the date of sampling, sex, length, and relative ages of the animals from which samples were collected for this study.

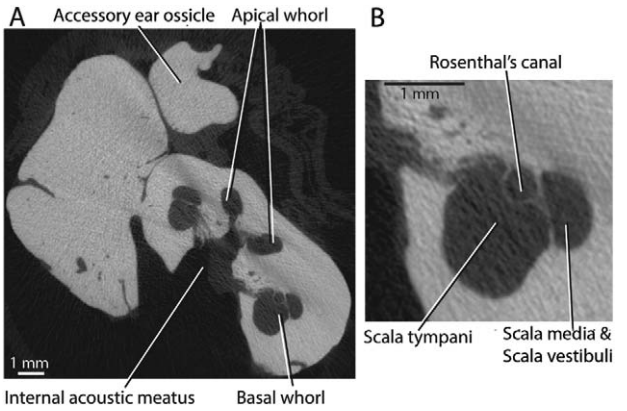


Fig. 1. *Delphinapterus leucas* microCT scan: (**A**) Representative midmodiolar microCT scan beluga whale 2012LDL7 Left. The accessory ossicle is an enlarged part of tympanic. (**B**) Enlarged view of Rosenthal's canal in the basal whorl of this section.

### MicroCT Scanning

We scan each periotic using a Scanco Medical vivaCT-75 scanner. Images are acquired at 70 kVp, 114 μA, and 200-ms integration time. Voxel size is 41 μm. We export scans in TIFF format to a work station and use Amira 5.4.1 to build three-dimensional (3D) images using the segmentation feature of Amira to image the relevant structures: the bony labyrinth and within it, Rosenthal's canal (Fig. 1). Approximately, 400 scans are used to build the complete bony labyrinth of one beluga. We use the reconstructed images in Amira to visualize the number of whorls in the cochlea and Rosenthal's canal (Fig. 2). Length measurements are taken in three dimensions on the Amira cochlear reconstruction to determine the specific length of these structures. This allows us to express positions along the cochlea as a percentage of total cochlear length.

### Rosenthal's Canal Assessment

We determine cross-sectional area of Rosenthal's canal using the apical view of the Amira 3D-reconstructed image in 9 or 10 locations along the cochlea, more or less equally-spaced. Each cross-sectional area is measured from an image produced by the "surface cut" feature of Amira. Using the rotate tool, we position the "surface cut" to be at a right angle to the canal's curvature (Fig. 2I). After a cut is made on the image by using the clip button, we create a new surface and visualize it using the "surface view" feature. We then toggle

*TABLE 1. Date of sampling, sex, length, and relative age of beluga whales used in this study*

| ID # | Date | Sex | Length (cm) | Age |
|---|---|---|---|---|
| 2010LDL8 | June 30, 2010 | Male | 356 | Adult |
| 2010LDL11 | June 30, 2010 | Female | 329 | Adult |
| 2010LDL12 | June 30, 2010 | Male | 318 | Adult |
| 2010LDL20 | June 30, 2010 | Male | 334 | Adult |
| 2010LDL21 | June 30, 2010 | Male | 364 | Adult |
| 2012LDL4 | July 9, 2012 | Female | 279 | Subadult |
| 2012LDL5 | July 9, 2012 | Male | 335 | Adult |
| 2012LDL7 | July 9, 2012 | Female | 280 | Subadult |
| 2012LDL9 | July 9, 2012 | Female | 317 | Subadult |
| 2013LDL7 | July 4, 2013 | Female | 368 | Adult |
| 2013LDL13 | July 4, 2013 | Male | 346 | Adult |
| 2013LDL15 | July 4, 2013 | Female | 153 | Near-term fetus |

Standard length—straight line measurement from snout to fork in the tail. Relative age based on color (white = adult; gray–white = subadult).

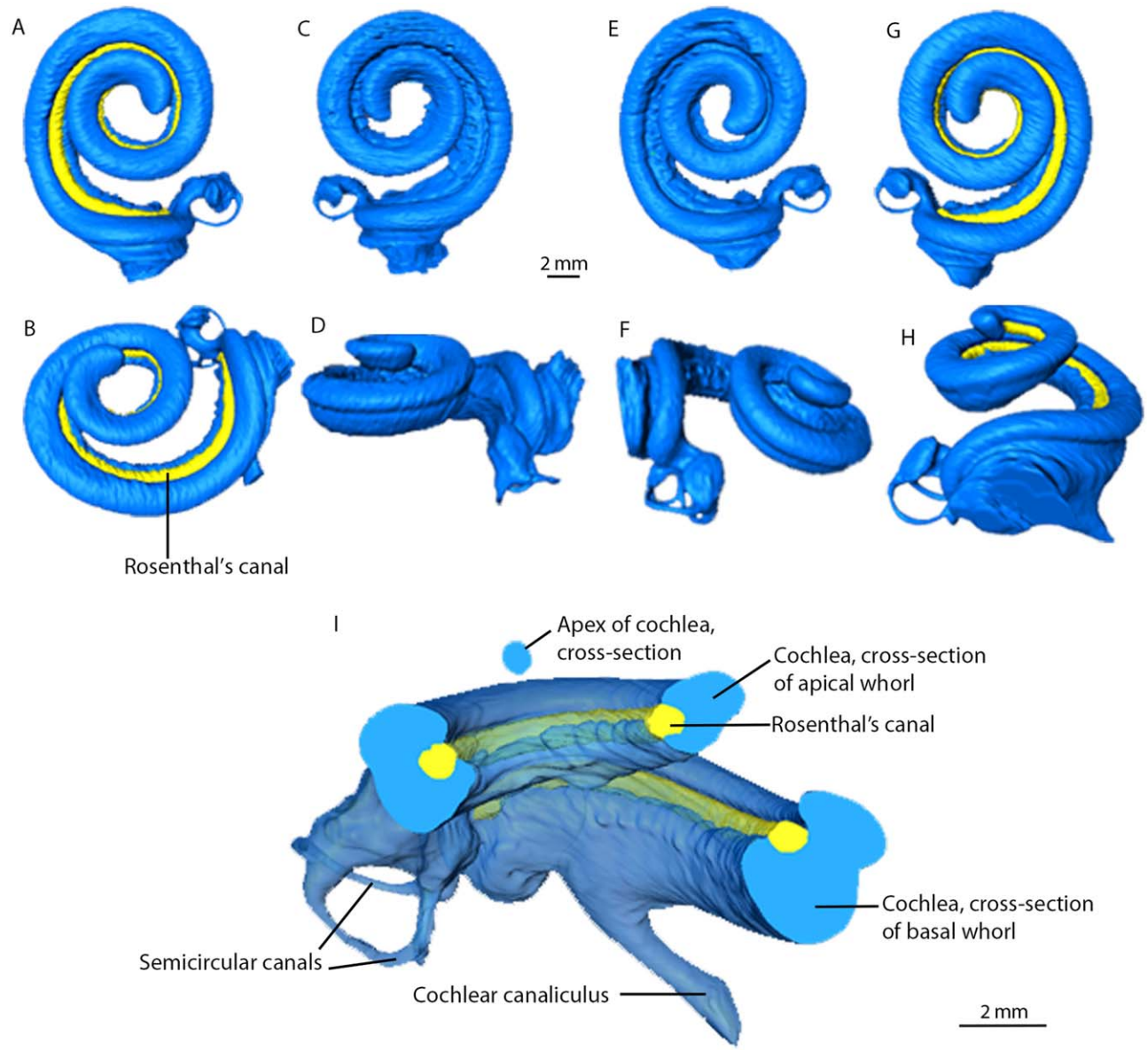


Fig. 2. *Delphinapterus leucas*, AMIRA3-D reconstructions of bony labyrinth based on microCT slices in blue, with Rosenthal's canal highlighted in yellow in some. Apical view (**A, C, E, G**), other representative views (**B, D, F, H**). Specimens used: 2010LDL11 left (A and B), 2013LDL8 right (C and D), 2012LDL4 left (E and F), and 2012LDL5 right (G and H). (**I**) AMIRA 3-D reconstruction of cochlea of 2010LDL11 left, cut virtually to show how cross-sectional areas of Rosenthal's canal were determined. Scale bar between C and E is for views A–H. Scale bar next to I is for view I.

off "surface cut" and "surface view," hiding all parts of the cochlea that were not in the surface cut. Using the "draw" button, we circle regions that we do not measure and remove these. We once again create a new surface on the appropriate cross-section and measure this surface area. Such measurements of cross-sectional areas based on CT-scans are more accurate than similar measurements on histological sections, because we avoided artifacts (shrinkage) associated with histological processing. We determined cross-sectional areas of Rosenthal's canal for eight beluga cochleas.

## Spiral Ganglion Dissection and Histology

Given that beluga cochleas are larger than those of most laboratory animals, we evaluated several methods of processing them (Fig. 3). Methods used in studies of small, perfused mammals (Wang et al., 2002; Ruijven et al., 2004) cannot be used to study our large specimens that could only be acquired after death. Hence, our specimens are immersion fixated.

For most specimens, we remove some of the bone with a Foredom microdrill to speed up the decalcification process. We immerse specimens in 10% Ethylenediaminetetraacetic acid (pH 7.5) for 3–6 weeks, renewing the solution after the first 2 weeks, testing occasionally for level of decalcification. This level of decalcification preserves the structural coherence of the cochlea, while making extraction of the organ of Corti and spiral ganglion possible. Subsequently, we use one of three methods, method three is the preferred method at present.

In the first method, we embedded some cochleas in araldite resin without initial removal of bone and cut them at 12μm on a

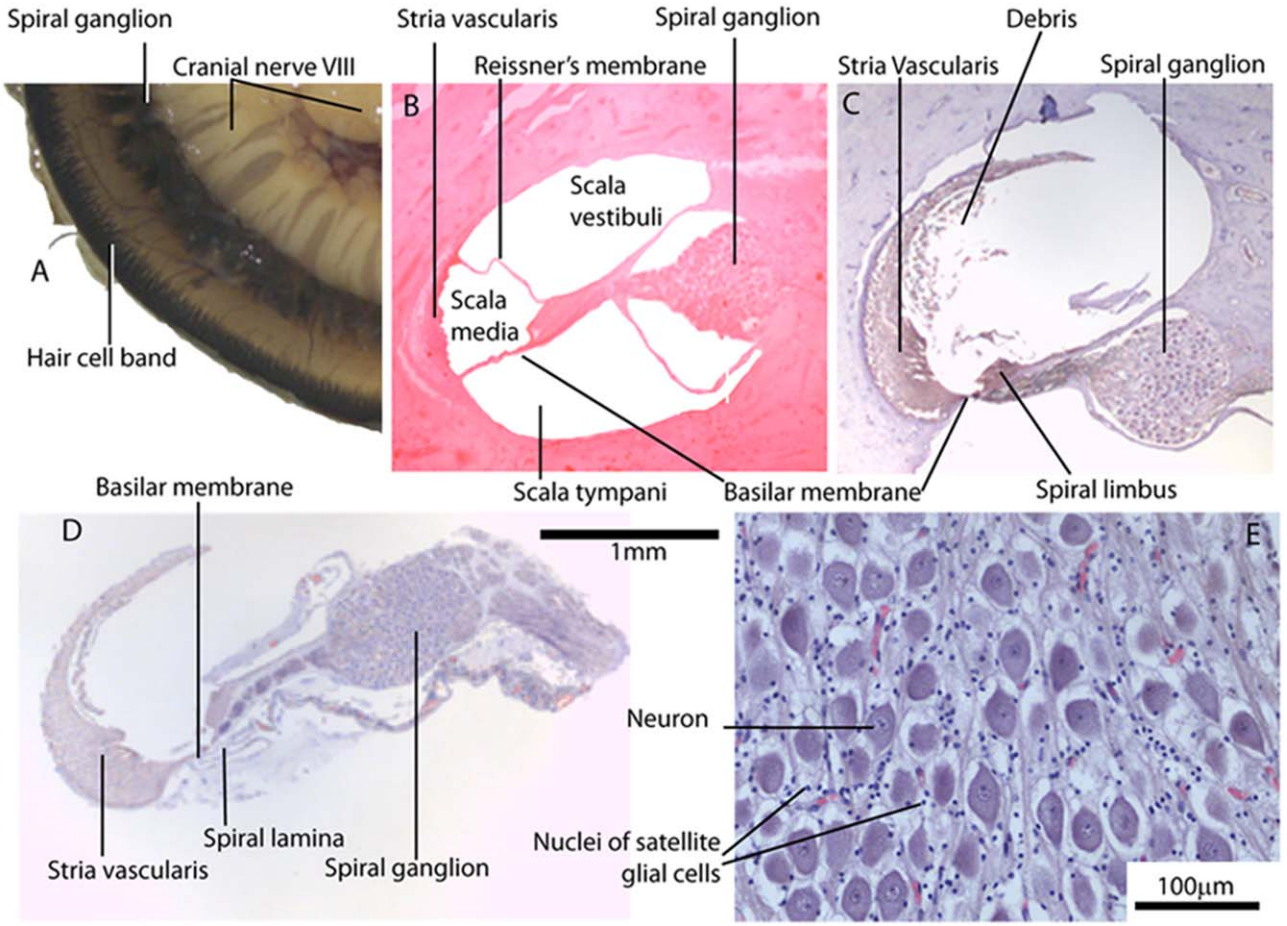


Fig. 3. *Delphinapterus leucas* specimen dissection and preparation: (**A**) Apical view of part of the cochlea during dissection; (**B**) Midmodiolar section of cochlea, where entire specimen was embedded in Araldite resin and stained with Eosin; (**C**) Midmodiolar section of cochlea, where entire specimen was paraffin embedded and stained with Hematoxylin and Eosin; (**D**) Excised specimen of organ of Corti and spiral ganglion stained with Hematoxylin and Eosin; (**E**) Enlarged area of spiral ganglion from D. Scale bar in center is for all images.

rotary microtome, staining them with eosin. These specimens preserve the internal anatomy, such as basilar and Reissner's membranes, well (Fig. 3B). Hair cells cannot be seen, either because of processing damage or as a result of blast damage at the time of death. Roberto et al. (1989) noted that exposure to gun shots at close range can result in immediate detachment of the organ of Corti, and indeed fragments of this organ are commonly found as debris in the scala media of our specimens.

In the second method, after decalcification, we embedded other entire cochleas in paraffin, cut them at 7 microns on a rotary microtome and stained with Hematoxtylin and Eosin. These display damage to the organ of Corti and often ruptured basilar and Reissner's membranes (Fig. 3C). Paraffin-embedded specimens do show well preserved cells in the spiral ganglion (Fig. 3E), allowing precise counting of spiral ganglion neurons over the entire length of the cochlea.

Most of our data were acquired using a third method. This method is modified from the dissection method of Johnsson and Hawkins (1967) for humans. For these specimens, after fixation but before decalcification, we flush 0.1% thionin through the scalae via the round and oval windows (Fig. 4), so that the cochlea can be seen through the bone during excess bone removal later on. Some specimens were flushed with 3% $OsO_4$ (Fig. 3A), but we found that this does not enhance resolution of the eventual sections. We then use a Foredom micro drill to remove excess bone, and provide access the scala vestibuli. Then, we decalcify the specimen using the method described above.

After decalcification, we dissect the organ of Corti and spiral ganglion under a dissection microscope using iris scissors and scalpels to remove excess decalcified bone. This opens the scala vestibuli. We remove pieces of the spiral ganglion with its adnexa, starting apically, and proceeding to the base. In some specimens only the spiral ganglion and Rosenthal's canal are extracted, whereas in others spiral lamina and stria are also included in the excised sample (Fig. 3D). The size of individual segment is mostly determined by the degree of curvature of the cochlea and our ability to handle small pieces of tissue with forceps. We map the position and size of each segment on a 3D-image that is based on the CT-scans and we refer to this diagram as the segment map (Fig. 5). Segments are dehydrated and embedded in paraffin, and the spiral ganglion segments area cut at right angles to the long axis of the ganglion, creating cross-sections. Sections are 7μm thick and are stained with hematoxylin and eosin. No thionin remains at this stage, but some spiral ganglia retain their $OsO_4$ staining (Fig. 6).

## Stereology

We use stereologic methods utilizing StereoInvestigator software (MicroBrightField, Williston, VT, version 10) to estimate the

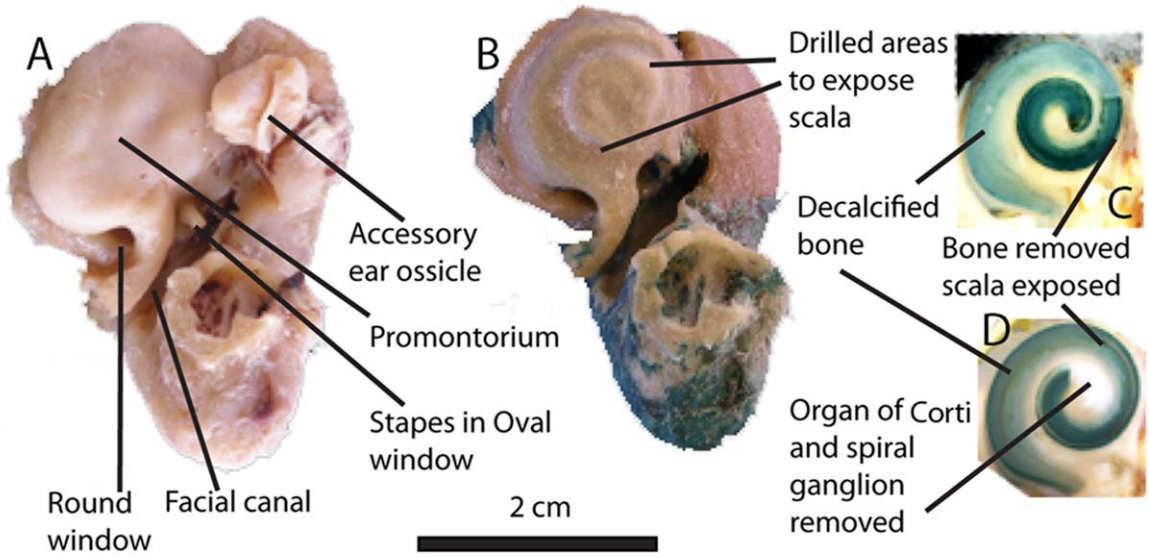


Fig. 4. *Delphinapterus leucas* petrosal (2013 LDL7 left) showing anatomy and different stages of dissection: (**A**) Bony specimen; (**B**) Specimen after thionin flush and excess bone removal; (**C**) Decalcified specimen with some bone removed and scala exposed; (**D**) Partially dissected specimen. Scale bar is for all images.

number of neurons in each segment of spiral ganglion, and use that estimate to assess neuron density of each cochlear segment. Although presumed Type I and Type II spiral ganglion cell bodies can be identified based on size and cytologic traits in cross section (Thomsen, 1966; Kellerhals et al., 1967; Spoendlin, 1972; Merck et al., 1977), differentiation among these falls outside of the scope of our research and we did not distinguish between these.

The set up includes an Olympus Bx-51 photomicroscope equipped with a Ludl XY motorized state, Heidenhain *z*-axis encoder, a digital camera, and a flat panel monitor to project images. Within a section, Rosenthal's canal is traced and all cells within it are counted using a computer assisted fractionator sampling scheme to count the nuclei. Neurons are counted at 40× magnification when the nucleus (diameter of 12.5 μm) is in focus, using a Counting Frame Width (*X* and *Y*) of 150 μm and a Sampling Grid (*X* and *Y*) of 150 μm. We do not use guard zones or the optical dissector of StereoInvestigator, because our sections are thin (7μm). The section evaluation interval is usually five (sometimes four or six), meaning we count every fifth (fourth or sixth) section. We usually count a total of five sections (sometimes four or six, once just three) to make up a data point in Figure 7B,C. The variation in evaluation interval or total number of sections counted resulted from our rejection of sections that were damaged due to processing and the number of sections available per slide.

We use the "Estimated Population using Mean Section Thickness from Sites with Counts" of StereoInvestigator to estimate neuron numbers per spiral ganglion subsegment. This method estimates the number of cells based on the operator (JDS) counting neurons in a number of "counting sites" (squares outlined on the screen) chosen by the program for each histological section. Section thickness is evaluated by the operator setting the top and bottom of each section at every fifth counting site as prompted by the program. These measured thicknesses are then averaged across the counted histological sections to give a "mean measured thickness value." "Counting sites" that do not contain marked objects are not included in this estimate.

This estimation process yields an approximation for the total number of neurons over the subsegment of the spiral ganglion segment studied. Usually each subsegment is 175 μm in length (when every fifth section is counted). We apply the Abercrombie correction as described by Konigsmark (1970) to avoid error due to cell splitting, following procedures used before for other cetaceans (Wever et al., 1971c). This gives us a final neuron number estimate for that sub-segment.

To standardize neuron estimates, we divided this number by subsegment length (175 μm in the above example). As such, we assume that the neurons per μm in each subsegment of the cochlea to be representative of the segment. We plot these estimates (neurons per μm) against the midpoint of each cochlear segment from base to apex (Fig. 7B). For example, if a cochlear segment was taken from 50 to 70% of cochlear length, its data point was plotted at 60%. Figure 7B, thus, shows estimates of neuron counts per cochlear segment and is not affected by cross-sectional area of Rosenthal's canal.

To estimate neuron density along the length of the cochlea, we take the estimated neuron counts within specific subsegments (as described above) and divide them by the total volume ($\mu m^3$) of that subsegment. Volumes are estimated in StereoInvestigator using the area of Rosenthal's canal, which is outlined by the operator, and the length of the subsegment. We plot these density estimates for each segment versus percent length along the cochlea from basal to apical (Fig. 7C).

Finally, we estimate the total neuronal count for the entire spiral ganglion based on calculated neuron count per linear micrometer for each subsegment. These neuron counts have to be multiplied by segment length to yield an estimate of a total neuron count per segment. We determined segment length based on measurements of the 3D-reconstructed CT-scans. Cell counts are based on histological images whereas the segment map is based on CT-scans before decalcification. Therefore, tissue shrinkage has to be taken into account in order for the total number of ganglion cells to be estimated. For one specimen (2013LDL15F, the left cochlea of a full-term fetus), we measure spiral ganglion segment length of the 10 excised preserved dissection specimens before and after histological processing. Postprocessing segment length is on average 88% (0.88) of its preprocessed length, with a standard deviation of 0.05. Using this, we estimate the postprocessing length of each spiral ganglion segment by multiplying segment lengths before decalcification by 0.88. This yields the length of the postprocessing segment. We multiply the number of neurons per μm within that segment (found above) by the postprocessed segment length to estimate the total number of neurons per segment.

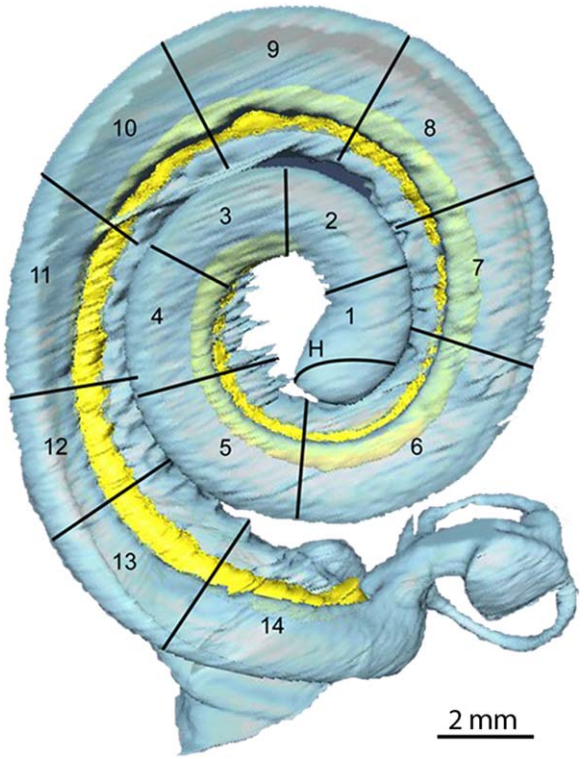


Fig. 5. *Delphinapterus leucas* segment map of labyrinth (2012LDL7 left) based on AMIRA 3D reconstruction of bony labyrinth (blue) and Rosenthal's canal (yellow) based on approximately 400 microCT scans: The size and location of Rosenthal's canal samples that were dissected out of this specimen are indicated by numbers. Each of these samples is a segment of Rosenthal's canal that is histologically processed and counted. H-Helicotrema.

We then, add all segment estimates together to obtain an overall neuron count for Rosenthal's canal.

## RESULTS

### Cochlear Morphometrics

We measured the length of the basilar membrane at the inner secondary spiral lamina, as well as Rosenthal's canal using the reconstructed 3D images in Amira. We determined that the cochlea of a beluga has 1.75–2 cochlear whorls, whereas Rosenthal's canal is shorter: between 1.5 and 1.75 whorls. The mean length of Rosenthal's canal is 37.2 mm (SD = 2.1 mm; $n = 10$, 2010LDL8 Left, 2010LDL8 Right, 2010LDL12 Right, 2010LDL11 Left, 2012LDL5 Right, 2012LDL9 Left, 2012LDL4 Right, 2012LDL7 Left, 2012LDL4 Left, and 2013LDL7 Left; Table 1). As would be expected, this is significantly shorter than the length of the basilar membrane (e.g., 2010LDL7 Left: 47.3 mm).

### Rosenthal's Canal

Figure 7A shows the variation in Rosenthal's canal cross-sectional area along its length. The cross-sectional surface area of Rosenthal's canal changes significantly and nonlinearly over the length of the cochlea with the largest areas found in the middle segment of the canal (Quadratic regression: $F_{2,77} = 40.022$, $P < 0.001$). Analysis of variance for percent length and individual ears further supports the interpretation of curvilinearity, and indicates that the cross-sectional area of Rosenthal's canal changes significantly along its length within individual ears (two-way Analysis of variance: $F_{47,25} = 11.54$, $P < 0.001$). There are also significant differences among individual ears (two way Analysis of variance: $F_{7,25} = 13.93$, $P < 0.001$) regardless of the position along the cochlea.

### Neuron Numbers of the Spiral Ganglion

Based on three specimens (2010LDL11 Left, 2012LDL7 Left, 2012LDL9 Left), we estimate that the mean total number of neurons in Rosenthal's canal of beluga whales is 234,504 (SD = 18,416). We also study distribution of neurons along the length of the cochlea, expressing "length" as a percent along the cochlear spiral, shown as the $x$-axis in Figure 7. We assess neural numbers in two different ways, as simple counts and as densities (Fig. 7B,C). We tested linear and quadratic models and found that, for simple counts, the quadratic regression $y = -0.001*\text{length}^2 + 0.091*\text{length} + 5.261$ shows a better fit than a linear model based on comparisons using AIC (Akaike Information Criterion) as a measure of relative quality of models for a given dataset, although it explains only a small fraction of the total variation in neuron counts (Quadratic regression: $F_{2,60} = 3.51$, $P = 0.036$, $R^2 = 0.11$). This indicates that the overall number of neurons per linear μm along the length of the cochlea more closely follows a curvilinear pattern than a straight line (Fig. 7B). Standardized regression coefficients indicate that both length and length$^2$ are weighted more than individuals, meaning that no single individual is driving the observed trend in neuron counts.

Figure 7C shows the variation of neuron density calculated by dividing neuron count by volume (as determined in StereoInvestigator). Neuron density here is defined as the number of neurons of a segment of the spiral ganglion divided by Rosenthal's canal volume for that segment (as determined from the histological sections).

### Histology of the Spiral Ganglion

Figure 6 shows representative histological sections of the spiral ganglion throughout the length of the cochlea of several individuals. Histological fixes and stains provide clear images, and neurons are easily counted. Neurons and their nuclei are easily visible as large cells, surrounded by small nuclei of accessory cells, and there are no features related to necrosis. Our method allows for the study of full or near cross-sections of the cochlea, in all regions. Neurons

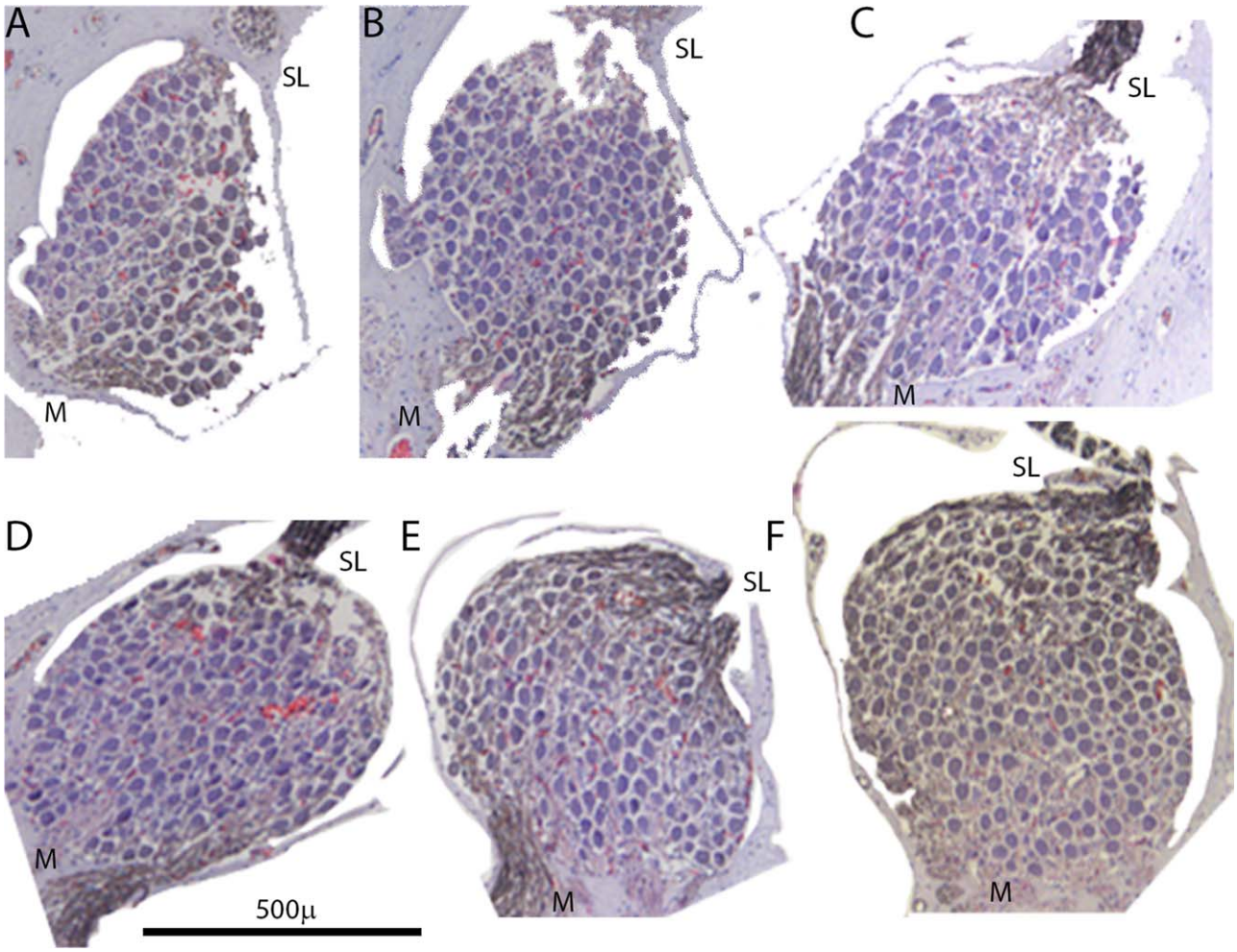


Fig. 6. *Delphinapterus leucas* spiral ganglion histological sections of specimen 2010LDL21 Right: Samples taken (**A**) 6% from base of spiral ganglion; (**B**) 19% from base; (**C**) 42% from base; (**D**) 67% from base; (**E**) 84% from base; (**F**) 89% from base. M indicates modiolar side, S indicates spiral lamina side. Scale bar for all images.

are distributed more or less evenly throughout each of the Rosenthal's canal sections, although there are fewer cell bodies peripherally, near the habenula perforata. This is the area where the intraganglionic spiral bundle is located.

## DISCUSSION

### Cochlear Morphometrics

Ketten (1984, 1991) distinguished two morphological types of odontocete cochleas: Type I cochleas are more-or-less flat and have fewer than two full whorls, while Type II cochleas are more cone shaped and have more than two full whorls. Wartzok and Ketten (1999) linked these to frequency specializations, stating that Type I species have peak hearing spectra above 100 kHz, and Type II have spectra below 80 kHz. The cochlea of the beluga (Fig. 2) is a loose spiral with less than two whorls that do not overlap, a shape characteristic of most nondelphinid odontocetes (Fleischer, 1976; Ketten, 1984). Beluga auditory evoked potentials suggest optimum sensitivity between 30 and 100 kHz (Klishin et al., 2000; Castellote et al., 2014). Thus, belugas are morphologically similar to Type I species, but functionally to Type II species, showing that intermediates between the Type I and Type II extremes occur.

Wever et al. (1971b, 1972) calculated basilar membrane length for several delphinids based on sectioned specimens [reconstructing them using Guild's method (1921)], and Ketten (1984, 1992) reported basilar membrane length for several cetaceans as "length of scalae" (Table 8 of Ketten, 1984). Ketten (1984, 1992) proposed that the length of the scalae and basilar membrane increase proportionately with body size in cetaceans. Our data are consistent with that hypothesis (Table 2).

### Rosenthal's Canal

Assessment of the size of Rosenthal's canal generally takes place in conjunction with studies that

*TABLE 2. Species, number of cochlear whorls, basilar membrane length (mm), and estimated spiral ganglion neuron number for several odontocete species*

| Species | Whorls (turns) | Basil memb | Spgang Neur | Ref |
|---|---|---|---|---|
| Delphinapterus leucas | 1.75–2 | 47.3 | 234,504 | |
| Monodon monoceros | 2–2.25 | | | 1,2 |
| Globicephala melaena | 2 | | | 3 |
| Delphinus delphis | 2.5 | | | 4 |
| Lagenorhynchus obliquidens | 1.75–2 | 29.5 | 50,412 | 5 |
| Lagenorhynchus albirostris | 2.25 | 34.9 | | 4 |
| Stenella attenuata | 2.5 | 36.9 | 82,506 | 4 |
| Stenella coeruleoalba | 2.5 | | | 4 |
| Stenella longirostris | 2.5 | | | 4 |
| Tursiops truncatus | 2–2.25 | 38.5 | 95,004 | 6 |
| Phocoena phocoena | 1.5 | 25.9 | 66,933 | 4 |
| Physeter catodon | 1.75–2 | 54 | | 1,7 |
| Inia geoffrensis | 1.5 | 38 | | 7 |

*Delphinapterus* data is from this study. (1) Hyrtl, 1845; (2) Pilleri et al. 1987; (3) Reysenbach de Haan, 1957; (4) Ketten, 1984; (5) Wever et al., 1972; (6) Wever et al., 1971a,b,c; (7) Ketten, 1992.

count spiral ganglion neurons in order to study neuron densities (Wicke and Firbas, 1970; Keithley and Feldman, 1979; Schuknecht, 1993; Dazert et al., 1996; Ruijven et al., 2004; Shepherd et al., 2005; Agterberg et al., 2010.) In our view, the number of neurons that serves a segment of the cochlear spiral is more important for hearing than how densely those neurons are packed. Johnson et al. (2011) showed that larger canal cross-sections match areas of higher neuron numbers in mice. This implies that two areas that have similar neuron densities may actually have very different neuron counts, and that studying densities would hide the spike in neuron counts. We tested this for beluga (Fig. 7A). Consistent with the observations for rodents (Johnson et al., 2011; Richter et al., 2011), our results indicate that the cross-sectional area of Rosenthal's canal of belugas varies along its length. This variation follows a similar path of increase and decrease in different individuals. Visually (Fig. 7A), it appears that cross-sectional area of Rosenthal's canal peaks near 20% to 70% of the length of the cochlea. In addition, the absolute cross-sectional area at any point along the length of the cochlea varies greatly between individuals, in some regions by as much as 50%.

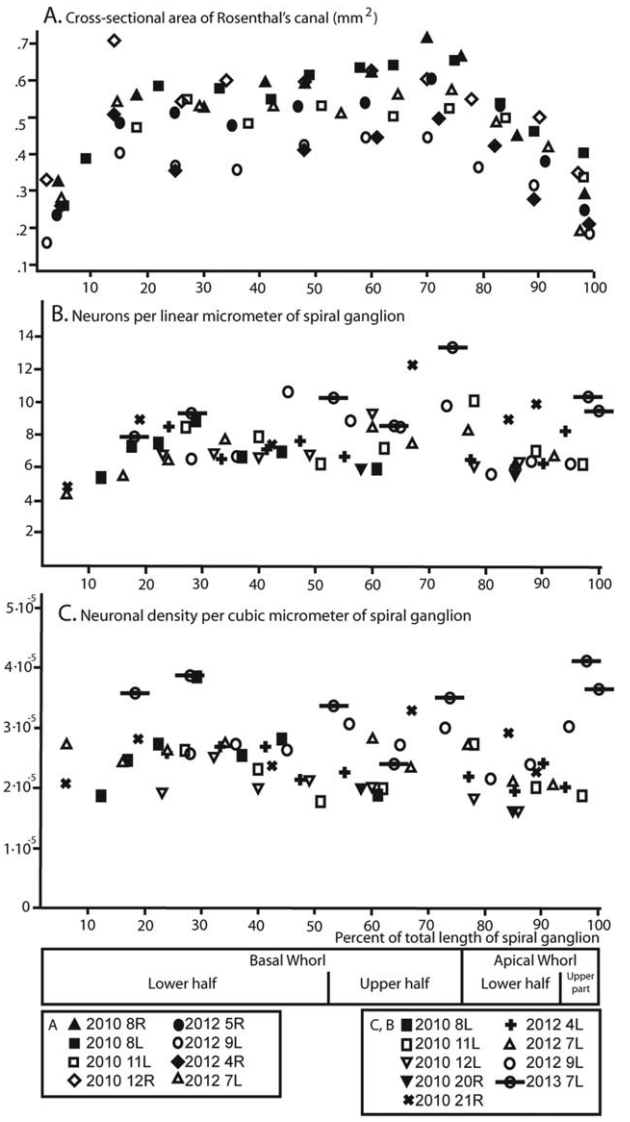


Fig. 7. *Delphinapterus leucas*, three variables of the spiral ganglion plotted against their position along the cochlea (x-axis, in percent of its length). (**A**) Cross-sectional areas of Rosenthal's canal based on CT data as analyzed by AMIRA; (**B**) Neuron numbers of the spiral ganglion, as determined for each cochlear segment based on counting multiple (usually five) histological sections; (**C**) Neuron densities of the spiral ganglion, calculated based on the data in B with cross-sectional areas of the histological sections that yielded those data. Specimen numbers for belugas omit the acronym LDL (see Materials and Methods for numbering convention).

## Neuron Numbers of the Spiral Ganglion

Table 2 compares estimates of total ganglion cell populations (neuron counts) for several odontocete species and uses only published data with well-documented estimation methods. Figure 8A shows that, in general, spiral ganglion number increases with body size, with the important exception that the Pacific white-sided dolphin, *Lagenorhynchus obliquidens*, has far fewer neurons than expected for its size. Consistent with its low neuron counts, *L. obliquidens* also has the shortest basilar membrane among the included delphinids (*Tursiops* and *Stenella*, Fig. 8B). Belugas also have relatively short basilar membranes given their size. It is not clear whether these minor differences are significant with regard to hearing, and it is possible that different estimation methods introduced some spurious effects in these results.

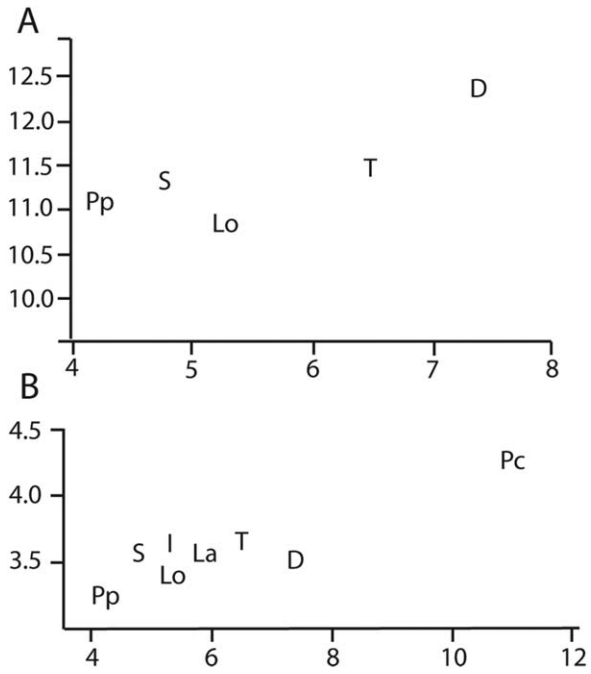


Fig. 8. *Delphinapterus leucas* (D, beluga), *Inia geoffrensis* (I, river dolphin), *Lagenorhynchus albirostris* (La, dolphin), *Lagenorhynchus obliquidens* (Lo, dolphin), *Phocoena phocoena* (Pp, porpoise), *Physeter catodon* (Pc, sperm whale), *Stenella attenuata* (S, dolphin), *Tursiops truncatus* (T, dolphin): Natural logarithm of spiral ganglion counts (**A**) and basilar membrane length (**B**) versus body weight for several cetaceans (see Table 2 for data, weight data from Jefferson et al., 2008) plotted against two cochlear variables.

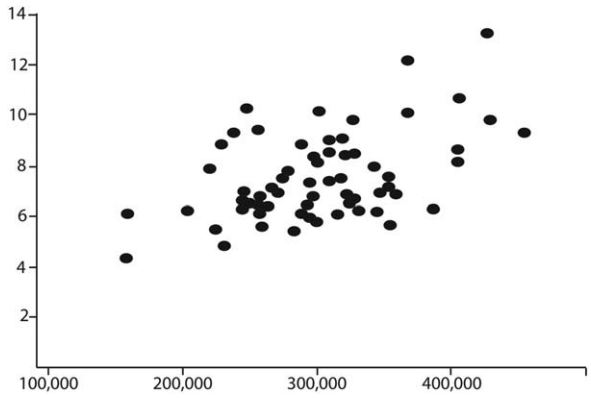


Fig. 9. *Delphinapterus leucas*, number of ganglion cells in segments of the spiral ganglion (*x*-axis) against mean histological cross-sectional area ($\mu m^2$) of that segment. Neuron number data from Figure 7B, area data as determined by StereoInvestigator.

Wever et al. (1971c) found that the neuron count of the dolphin *T. truncatus* spiral ganglion is not constant along the length of the cochlea, consistent with recent findings in rodents (Johnson et al., 2011; Richter et al., 2011). For beluga, the data points of Figure 7B significantly fit a quadratic curve. Age has been shown to affect neuron counts in other mammals (Keithley and Feldman 1979; Schuknecht, 1993; Richter et al., 2011). The two youngest individuals in our sample (based on their gray-white skin color, Jefferson et al., 2008) are 2012LDL4 and 2012LDL7, whereas 2010LDL21 is white and, therefore, older (Brodie et al., 2013). Data points for the two young individuals are low within the data envelop of Figure 7B, whereas the older whale is high in that distribution, the opposite of what would be expected if age induced hearing loss was present.

Given that Figure 7A is similar in shape, we suggest that cross-sectional diameter of Rosenthal's canal and cell counts are correlated. In Figure 9, we plotted spiral ganglion numbers against mean histological cross-sectional areas of Rosenthal's canal within the same subsegment, using the same data collected for Figure 7B,C. This figure shows that there is a clear correlation between Rosenthal's canal cross-sectional area, and number of neurons. This would mean that density (the quotient of neuron number and cross-sectional area) does not capture functional differences in variation of neuron numbers serving different segments of the cochlea.

To evaluate this effect, we calculated neuron densities (Fig. 7C). Density estimates are useful when comparing similar areas of the cochlea among comparable animals (such as animals of the same age with different levels of hearing damage), but we are interested in variability along the cochlea of individuals. The variation in Rosenthal's canal cross-sectional area may introduce a significant effect.

### Histology of the Spiral Ganglion

Damage to the spiral ganglion can be the result of acoustic trauma: exposure of hair cells to high intensity sounds (Schuknecht, 1993; Hurley et al., 2007; Henderson et al., 2008). When such exposure takes place in a limited frequency range, damage to the hair cells and associated spiral ganglion cells is often limited to a specific part of the cochlea, and neuron densities in this area will be lower than in adjacent, healthy areas. Histologically, we observed no areas of low spiral ganglion cells (Fig. 6), and this supports the qualitative findings on the cell counts (Fig. 7B). This is consistent with the interpretation that, using our method, no spiral ganglion damage in this group of belugas can be detected.

## CONCLUSIONS

We studied a sample of wild-caught, healthy beluga whales, and gathered baseline information on cochlea and spiral ganglion. Beluga cochlear shape is similar to that of other odontocetes, but does not fit well in the traditionally distinguished categories of odontocete cochleas as defined by Ketten (1984) and Wartzok and Ketten (1999). We

studied Rosenthal's canal cross-sectional areas and found these to vary along the cochlea, having two local maxima. Similarly, spiral ganglion neuron counts vary in different segments of the cochlea. We studied simple neuron counts, as well as densities (counts/cross-sectional areas). In our opinion, studying simple neuron counts along with cross-sectional areas of Rosenthal's canal captures some aspects of functional variation of the spiral ganglion along the cochlea, whereas neuron density measures do not in this cetacean.

Histological assessment and neuron cell counts suggest that there is no evidence for auditory damage to the spiral ganglion of these beluga ears.

## ACKNOWLEDGMENTS

The authors would like to thank the hunters and residents of Point Lay and the Alaska Beluga Whale Committee for allowing sampling of whales. The study would not have been possible without their trust and support. A number of people with the North Slope Borough, Department of Wildlife Management (NSB-DWM) provided a variety of assistance to make this project successful, including, Malissa Langley, Janell Kaleak, Molly Spicer, Lucia Johnston, and Bobby Sarren. NSB-DWM Director Taqulik Hepa was especially supportive of this project. The authors thank Gary Rose, Cyrus Kellermier, Madiha Khan, and Colleen Waickman for their assistance in sample processing and data collection. The authors thank Michael Macrander and Koen Broker for comments on the manuscript.

## LITERATURE CITED

Abrashkin KA, Izumikawa M, Miyazawa T, Wang C, Crumling MA, Swiderski DL, Beyer LA, Gong TL, Raphael Y. 2006. The fate of outer hair cells after acoustic or ototoxic insults. Hear Res 218:20–29.

Agterberg MJH, Versnel H, de Groot JCMJ, van den Broek M, Klis SFL. 2010. Chronic electrical stimulation does not prevent spiral ganglion cell degeneration in deafened guinea pigs. Hear Res 269:169–179.

Au WWL, Penner RH, Turl CW. 1988. Propagation of beluga echolocation. In: Nachtigall PE, Moore PWB, editors. Animal Sonar: Processes and Performance. New York, NY: Plenum Press. pp 47–51.

Bel'kovitch VM, Sh'ekotov MN. 1990. The Belukha Whale: Natural Behavior and Bioacoustics. Moscow: USSR Academy of Sciences. Translated by Wood's Hole Oceanographic Institution, 1993, 115 p., 49 figs.

Brodie P, Ramirez K, Haulena M. 2013. Growth and maturity of belugas (*Delphinapterus leucas*) in Cumberland Sound, Canada, and in captivity: Evidence for two growth layer groups (GLGs) per year in teeth. J Cetacean Res Manag 13: 1–18.

Castellote M, Mooney TA, Quakenbush L, Hobbs R, Goertz C, Gaglione E. 2014. Baseline hearing abilities and variability in wild beluga whales (*Delphinapterus leucas*). J Exp Biol 217: 1682–1691.

Dazert S, Feldman ML, Keithley EM. 1996. Cochlear spiral ganglion cell degeneration in wild-caught mice as a function of age. Hear Res 100:101–106.

Finneran JJ, Belting T, McBain J, Dalton L, Ridgway SH. 2005. Pure tone audiograms and possible aminoglycoside-induced hearing loss in belugas (*Delphinapterus leucas*). J Acoust Soc Am 117:3936–3943.

Firbas W, Wicke W, Volavsek C. 1970. Über Zahl und Anordnung der Ganglienzellen im Ganglion spirale des Meerschweinchens. Monatsschr Ohrenheilkd Laryngorhinol 104:241–246.

Fleischer G. 1976. Hearing in extinct cetaceans as determined by cochlear structure. J Paleontol 50:133–152.

Fredelius L. 1988. Time sequence of degeneration pattern of the organ of Corti after acoustic overstimulation. A transmission electron microscopy study. Acta Otolaryngol 106: 373–385.

Fredelius L, Rask-Andersen H, Johansson B, Urquiza R, Bagger-Sjöbäck D, Wersäll J. 1988. Time sequence of degeneration pattern of the organ of Corti after acoustic stimulation. Acta Otolaryngol 106:81–93.

Gao G, Zhou K, 1991. The number of fibers and range of fiber diameters in the cochlear nerve of three odontocete species. Can J Zool 69:2360–2364.

Henderson D, Hu B, Bielefeld E. 2008. Patterns and mechanisms of noise-induced cochlear pathology. In: Schacht J, Popper AN, Fay RR, editors. Auditory Trauma, Protection, and Repair. New York, NY: Springer. pp 195–217.

Hurley PA, Crook JM, Shepherd RK. 2007. Schwann cells revert to non-myelinating phenotypes in the deafened rat cochlea. Eur J Neurosci 26:1813–1821.

Hyrtl J. 1845. Vergleichend anatomische Untersuchungen über das innere Gehörogan des Menschen und der Säugethiere. Prag: Friedrich Ehrlich. 139 p.

Jansen J, Jansen JKS. 1969. The nervous system of cetacean. In: Andersen HT, editor. The Biology of Marine Mammals. New York, NY: Academic Press. pp 175–252.

Jefferson TA, Webber MA, Pitman RL. 2008. Marine Mammals of the World: A Comprehensive Guide to their Identification. Amsterdam: Elsevier. 573 p.

Johnson SB, Schmitz HM, Santi PA. 2011. TSLIM imaging and a morphometric analysis of the mouse spiral ganglion. Hear Res 278:34–42.

Johnsson LG, Hawkins JE Jr. 1967. A direct approach to cochlear anatomy and pathology in man. Arch Otolaryngol 85: 599–613.

Keithley EM, Feldman M. 1979. Spiral ganglion cell counts in an age-graded series of rat cochleas. J Comp Neurol 188: 429–442.

Kellerhals B, Engström H, Ades HW. 1967. Die Morphologie des Ganglion spirale cochleae. Acta Otolaryngol 64(suppl 226):5–78.

Ketten DR. 1984. Correlations of Morphology with Frequency for Odontocete Cochlea: Stystmatics and Topology [dissertation]. Baltimore, MD: The Johns Hopkins University. 349 p. Available from: University Microfilms International, Ann Arbor, MI; 8501651.

Ketten DR. 1991. The marine mammal ear: specializations for aquatic audition and echolocation. In: Webster DB, Fay RR, Popper AN, editors. The Evolutionary Biology of Hearing. New York, NY: Springer-Verlag. pp 117–750.

Ketten DR. 1992. The cetacean ear: Form, frequency, and evolution. In: Thomas J, Kastelein RA, Supin AY, editors. Marine Mammal Sensory Systems. New York, NY: Plenum Press. pp 53–75.

Ketten DR. 1997. Structure and function in whale ears. Bioacoustics 8:103–135.

Klishin VO, Popov VV, Supin AY. 2000. Hearing capabilities of a beluga whale, *Delphinapterus leucas*. Aquat Mamm 26: 212–228.

Konigsmark BW. 1970. Methods for the counting of neurons. In: Nauta WJH, Ebbesson SOE, editors. Contemporary Research Methods in Neuroanatomy. New York, NY: Springer-Verlag. pp 315–340.

Lurie MH, Davis H, Hawkins JE Jr.1944. Acoustic trauma of the organ of corti in the guinea pig. Laryngoscope 54:375–386

Merck W, Riede UN, Löhle E, Cürten I. 1977. Eine ultrastrukturell-morphometrische analyse des ganglion spirale cochleae de Meerschweinchens. Arch Otorhinolaryngol 214:303–312.

Morgane PJ, Jacobs MS. 1972. Comparative anatomy of the cetacean nervous system. In: Harrison RJ, editors. Functional Anatomy of Marine Mammals, Vol. 1. New York, NY: Academic Press. pp 117–244.

O'Corry-Crowe GM. 2009. Beluga whale: *Delphinapterus leucus*. In: Perrin WF, Würsig B, Thewissen JGM, editors. Encyclopedia of Marine Mammals, 2nd ed. Boston, MA: Elsevier. pp 108–112.

Ohlemiller KK, Wright JS, Heidbreder AF. 2000. Vulnerability to noise-induced hearing loss in 'middle-aged' and young adult mice: A dose-response approach in CBA, C57BL, and BALB inbred strains. Hear Res 149:239–247.

Pilleri G, Gihr M, Kraus C. 1987. The Organ of Hearing in Cetacea: I. Recent Species. Berne: Brain Anatomy Institute. 127 p.

Reysenbach de Haan FW. 1957. Hearing in whales. Acta Otolaryngol Suppl 134:1–114.

Richter CP, Kumar G, Webster E, Banas SK, Whitlon DS. 2011. Unbiased counting of neurons in the cochlea of developing gerbils. Hear Res 278:43–51.

Roberto M, Hamernik RP, Turrentine GA. 1989. Damage of the auditory system associated with acute blast trauma. Ann Otol Rhinol Laryngol 98(suppl 140):23–34.

Ruijven MWv, Groot JCd, Smoorenburg GF. 2004. Time sequence of degeneration pattern in the guinea pig cochlea during cisplatin administration. A quantitative histological study. Hear Res 197:44–54.

Shepherd RK, Coco A, Epp SB, Crook JM. 2005. Chronic depolarization enhances the trophic effects of brain-derived neurotrophic factor in rescuing auditory neurons following a sensorineural hearing loss. J Comp Neurol 486:145–158.

Schuknecht HF. 1993. Pathology of the Ear, 2nd ed. Philadelphia: Lea & Febiger. 672 p.

Solntseva GN. 2007. Morphology of the Auditory and Vestibular Organs in Mammals, with Emphasis on Marine Species. Boston: Pensoft Publishers & Brill Academic Publishers. 243 p.

Spoendlin H. 1972. Innervation densities of the cochlea. Acta Otolaryngol 73:235–248.

Stocker M. 2011. Noisy oil exploration disrupts marine life. Nature 473:285.

Thomsen E. 1966. The ultrastructure of the spiral ganglion in the guinea pig. Acta Otolaryngol 63(suppl 224):442–448.

Vergara V, Barrett-Lennard LG. 2008. Vocal development in a beluga calf (*Delphinapterus leucas*). Aquat Mamm 34:123–143.

Wang Y, Hirose K, Liberman MC. 2002. Dynamics of noise-induced cellular injury and repair in the mouse cochlea. J Assoc Res Otolaryngol 3:248–268.

Wartzok D, Ketten DR. 1999. Marine mammal sensory systems. In: Reynolds III JE, Rommel SA, editors. Biology of Marine Mammals. Washington DC: Smithsonian Institution Press. pp 117–175.

Wever EG, McCormick JG, Palin J, Ridgway SH. 1971a. The cochlea of the dolphin, *Tursiops truncatus*: General morphology. Proc Natl Acad Sci USA 68:2381–2385.

Wever EG, McCormick JG, Palin J, Ridgway SH. 1971b. The cochlea of the dolphin, *Tursiops truncatus*: The basilar membrane. Proc Natl Acad Sci USA 68:2708–2711.

Wever EG, McCormick JG, Palin J, Ridgway SH. 1971c. The cochlea of the dolphin, *Tursiops truncatus*: Hair cells and ganglion cells. Proc Natl Acad Sci USA 68:2908–2912.

Wever EG, McCormick JG, Palin J, Ridgway SH. 1972. Cochlear structure in the dolphin, *Lagenorhynchus obliquidens*. Proc Natl Acad Sci USA 69:657–661.

Wicke VW, Firbas W. 1970. Quantitative untersuchungen am ganglion spirale des meerschweinchens nach lärmbelastung. Monatsschr Ohrenheilkd Laryngorhinol 104:433–440.